Measurement Based Throughput Evaluation of Residual Frequency Offset Compensation in WiMAX

Qi Wang, Sebastian Caban, Christian Mehlführer and Markus Rupp
Institute of Communications and Radio-Frequency Engineering
Vienna University of Technology, Gusshausstrasse 25/389, A-1040 Vienna, Austria
Email: {*qwang, scaban, chmehl, mrupp*}*@nt.tuwien.ac.at*

Abstract - *WiMAX utilizes a physical-layer based on OFDM that is very sensitive to carrier frequency offset. Even though most of this offset can be compensated using the initial training sequence, there still remains a residual frequency offset due to estimation errors. The methods proposed to correct for this remaining offset are mostly tested by means of pure simulation.*
In this work, we present outdoor-to-indoor WiMAX measurements in an alpine scenario in which four residual frequency offset compensation schemes are investigated. We evaluate the performance of these schemes in terms of measured throughput rather than only frequency offset estimation error. If a-priori knowledge of the previous receive frame is exploited in a symbol-wise frequency offset estimator, the measurement results show worse performance than simulations predict. Consistent with simulations, the data-aided method effectively compensates the throughput loss due to the residual frequency offset.

Keywords - *Residual Frequency Offset Compensation, WiMAX, Measurement*

1. INTRODUCTION

Carrier frequency synchronization is a crucial issue for OFDM based WiMAX since the Carrier Frequency Offset (CFO) introduces inter-carrier interference. Numerous papers dealing with carrier frequency synchronization in OFDM can be found (e.g. [1–3]). The basic idea is to split the CFO into the Fractional Frequency Offset (FFO), the Integer Frequency Offset (IFO) and the Residual Frequency Offset (RFO). For WiMAX, the FFO and the IFO are estimated and corrected using the preamble at the beginning of each frame. To estimate the RFO during the data transmission, pilot-based and decision directed methods have been developed [2, 3] and improved [4]. To the authors' knowledge, however, all evaluations presented in literature are based on simulations.

In this work, we measure a WiMAX transmission with CFO in a realistic alpine scenario. Four RFO compensation schemes are evaluated. The results are based on outdoor-to-indoor measurements utilizing the Vienna MIMO testbed [5, 6].

2. RESIDUAL FREQUENCY OFFSET COMPENSATION IN WIMAX

In this section, we first introduce the basic idea of RFO estimation. Then we review the four RFO compensation schemes utilized in the measurement, namely the pilot-based frame-wise approach, the pilot-based symbol-wise approach, the symbol-wise approach with pre-knowledge and the data-aided approach [4].

2.1. System Model

In an OFDM system, the CFO Δf_{CFO} is normalized to the subcarrier spacing f_{s} and denoted by $\varepsilon_{\text{CFO}} = \frac{\Delta f_{\text{CFO}}}{f_{\text{s}}}$. After the FFO and the IFO are corrected, the RFO is typically in the order of 10^{-3}.

In the following, we denote the OFDM symbol index within one frame by l, the receive antenna index by m, the subcarrier index by k, the FFT size by N and the Cyclic Prefix (CP) length by N_{g}. The received symbol in the frequency domain is referred to as $R_{l,k}^{(m)}$, the transmitted symbol as $X_{l,k}^{(m)}$, the channel frequency response as $H_{l,k}^{(m)}$ and the additive Gaussian noise as $V_{l,k}^{(m)}$. According to [2, 4], the RFO can be derived from the phase variation $j2\pi\tilde{\varepsilon}_{\text{RFO}}$ in two consecutive OFDM symbols using

$$\begin{aligned} W_{l,k}^{(m)} &= R_{l-1,k}^{(m)} R_{l,k}^{(m)*} (X_{l-1,k}^{(m)} X_{l,k}^{(m)*})^* \\ &= (H_{l-1,k}^{(m)} X_{l-1,k}^{(m)} + V_{l-1,k}^{(m)}) \\ &\quad \cdot (H_{l-1,k}^{(m)} X_{l,k}^{(m)} e^{j2\pi\tilde{\varepsilon}} + V_{l,k}^{(m)})^* (X_{l-1,k}^{(m)} X_{l,k}^{(m)*})^* \\ &= |H_{l-1,k}^{(m)}|^2 |X_{l-1,k}^{(m)}|^2 |X_{l,k}^{(m)}|^2 e^{-j2\pi\tilde{\varepsilon}_{\text{RFO}}} + \tilde{V}_{l,k}^{(m)} \end{aligned} \tag{1}$$

which leads to the estimated RFO $\varepsilon_{\text{RFO}} = \tilde{\varepsilon}_{\text{RFO}} \cdot N/(N + N_{\text{g}})$. The additional noise terms are contained in $\tilde{V}_{l,k}^{(m)}$.

2.2. Pilot-based Frame-wise Approach

Assuming N_{R} receive antennas, we denote the subset of pilot subcarrier indices by $\mathcal{N}_{\text{p}}$ and the total number of OFDM symbols in one frame by N_{f}. The estimated RFO can be derived by averaging over N_{f} OFDM symbols in the current frame. This yields the estimated RFO

$$\hat{\varepsilon}_{\text{RFO, Frame}} = -\frac{1}{2\pi} \frac{N}{N + N_{\text{g}}} \arg \left\{ \sum_{l=2}^{N_{\text{f}}} \sum_{m=1}^{N_{\text{R}}} \sum_{k \in \mathcal{N}_{\text{p}}} W_{l,k}^{(m)} \right\}. \tag{2}$$

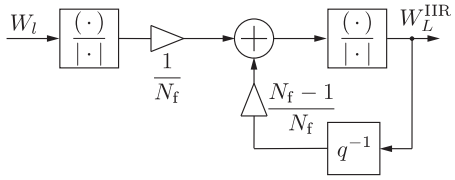

Fig. 1. IIR filter for averaging

From the practical point of view, this approach has the drawback that the complete data-frame has to be stored until the first estimate of the RFO is obtained.

2.3. Pilot-based Symbol-wise Approach

In order to produce an instantaneous estimate at each OFDM symbol, an alternative is to combine the results of the first L received OFDM symbols in the current frame. In this way, the estimated RFO at the L-th OFDM symbol in the current frame is given by

$$\hat{\varepsilon}_{\mathrm{RFO},L} = -\frac{1}{2\pi}\frac{N}{N+N_\mathrm{g}}\arg\left\{\sum_{l=2}^{L}\sum_{m=1}^{N_\mathrm{R}}\sum_{k\in\mathcal{N}_\mathrm{p}} W_{l,k}^{(m)}\right\}. \tag{3}$$

The estimation window is initialized at the beginning of each frame and then grows during the transmission. Starting from a "zero" phase, the estimation result is updated and improved at every newly received OFDM symbol.

2.4. Symbol-wise Approach with Pre-knowledge

In order to avoid the "zero start" phase, the symbol-wise approach with pre-knowledge introduced in [4] is considered. Since the two frames have different FFO and IFO estimates, the following initial RFO is assumed

$$\hat{\varepsilon}_{\mathrm{RFO},1}^{\mathrm{initial}} = \hat{\varepsilon}_{\mathrm{RFO},N_\mathrm{f}}^{\mathrm{previous}} + \hat{\varepsilon}_{\mathrm{FFO}}^{\mathrm{previous}} + \hat{\varepsilon}_{\mathrm{IFO}}^{\mathrm{previous}} - \hat{\varepsilon}_{\mathrm{FFO}}^{\mathrm{current}} - \hat{\varepsilon}_{\mathrm{IFO}}^{\mathrm{current}}. \tag{4}$$

The corresponding initial W_1 at the first OFDM symbol in the current frame is expressed as

$$W_1 = \exp\left\{-j2\pi\varepsilon_{\mathrm{RFO},1}^{\mathrm{initial}}\cdot\frac{N+N_\mathrm{g}}{N}\right\}. \tag{5}$$

At each OFDM symbol, the newly generated W_l goes into an IIR filter as shown in Fig. 1. The new value is weighted by $\frac{1}{N_\mathrm{f}}$ and the stored one weighted by $\frac{N_\mathrm{f}-1}{N_\mathrm{f}}$. The RFO for the L-th OFDM symbol is derived as

$$\hat{\varepsilon}_{\mathrm{RFO},L} = -\frac{1}{2\pi}\frac{N}{N+N_\mathrm{g}}\arg\left\{W_L^{\mathrm{IIR}}\right\}. \tag{6}$$

2.5. Data-aided Approach

In this section, the data-aided method with optimal combining factors introduced in [4] is briefly reviewed. The block diagram is shown in Fig. 2. In the *RFO Estimation* block in the upper branch, the RFO at the OFDM

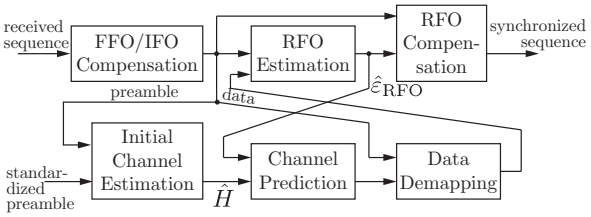

Fig. 2. Data-aided residual frequency offset estimation

symbol L in the current frame is derived as

$$\hat{\varepsilon}_{\mathrm{DA},L} = -\frac{1}{2\pi}\frac{N}{N+N_\mathrm{g}}\arg\left\{\sum_{l=2}^{L}\sum_{m=1}^{N_\mathrm{R}}\sum_{k\in\mathcal{N}} g_{l,k}W_{l,k}^{(m)}\right\}. \tag{7}$$

The pilot and data subcarrier indices required for the combining are contained in $\mathcal{N}$. The optimal weighting factors $g_{l,k}$ according to [4] are given by

$$g_{l,k} = \frac{1}{|\hat{X}_{l-1,k}|^2 + |\hat{X}_{l,k}|^2}, \tag{8}$$

where $\hat{X}_{l,k}$ denotes the demapped data symbol. For demapping, an initial channel estimation is required at the beginning of each frame. The channel frequency response in the L-th OFDM symbol of one frame can be predicted by

$$\hat{H}_{L,k}^{(m)} = \hat{H}_{L-1,k}^{(m)}\exp\left\{j2\pi\hat{\varepsilon}_{\mathrm{DA},L-1}\cdot\frac{N+N_\mathrm{g}}{N}\right\}. \tag{9}$$

Using this predicted channel frequency response, the data symbols are hard demapped and fed into the *RFO Estimation* block.

3. MEASUREMENT SETUP

In the following, we will report on WiMAX measurements that were carried out during September 2008 in the Austrian "Drautal"-valley. The RX unit was set up inside a house on one side of the valley. The base station was placed 5.7 km away from the RX unit on the other side of the valley (see Fig. 3). Google Earth coordinates of the measurement setup can be found at [7].

At a center frequency of 2.5 GHz, we transmitted SISO WiMAX data blocks at 9 different transmit power levels, 10 different receiver local oscillator frequencies and 110 different positions of the RX antennas[1]. The frequency adjustable local oscillator of the receiver was synchronized[2] to the local oscillator of the transmitter with a relative accuracy of 10^{-4} ppm. In addition, the baseband-hardware clock of the transmitter and the receiver were locked to the same reference, that is, only the local oscillator frequency has been changed accurately in order to allow for measuring oscillator offsets from 0.001 MHz to 0.5 MHz. More details on the measurement setup can be found in [6].

[1] uniformly distributed within an area of 3×3 wavelengths

[2] We utilize a GPS receiver, a Rubidium Frequency Standard, and a phase locked local oscillator at the TX and the RX unit.

Table 1. CFOs in MHz, ppm, and subcarrier spacing

CFOs in MHz	0.001	0.002	0.005	0.01	0.02
in ppm	0.41	0.82	2.06	4.11	8.22
subcarrier spacing	0.04	0.08	0.2	0.41	0.82
CFOs in MHz	0.05	0.1	0.2	0.5	
in ppm	20.55	41.1	82.2	205.51	
subcarrier spacing	2.05	4.1	8.2	20.49	

4. MEASUREMENT RESULTS

In this section, measurement results are presented. We first expose the behavior of the estimators in reality, then evaluate the four RFO compensation schemes described in Section 2.

4.1. Evaluation Procedure

Similar as in the WiMAX standard [8], the sampling frequency is set to 6.25 MHz, resulting in a subcarrier spacing of 24.4 kHz. In Table 1, the nine introduced CFOs are displayed in terms of ppm and normalized subcarrier spacing. Correct symbol timing is ensured by the hardware synchronization of the testbed. The FFO and the IFO are corrected using the method described in [2]. The four RFO compensation approaches in Section 2 are implemented.

In order to evaluate the physical-layer throughput, the method in [9] is used. Note that we did *not* change the RX antenna position between measuring the seven adaptive modulation and coding (AMC) schemes, the nine different transmit power levels and the nine different CFOs. The AMC feedback is assumed to be optimal, that is, the AMC scheme that achieves the largest throughput for a specific channel realization at a specific transmit power is selected. Only the number of bits in correctly received frames is counted in the throughput evaluation.

4.2. Estimator Behavior

In this section, we take the pilot-based frame-wise RFO estimator as an example to show its basic characteristics in reality.

Fig. 4 shows the throughput curves of the nine compensated CFO levels. Except the one from the largest CFO of 205.51 ppm, the curves stay closely to each other. This is well in agreement with the analytical result in [3] which states that the estimation error is independent of the CFO. Therefore, in the later throughput evaluation, we take the average throughput of the nine cases.

To discover the relationship between the estimation error and the transmit power, the Mean Square Error

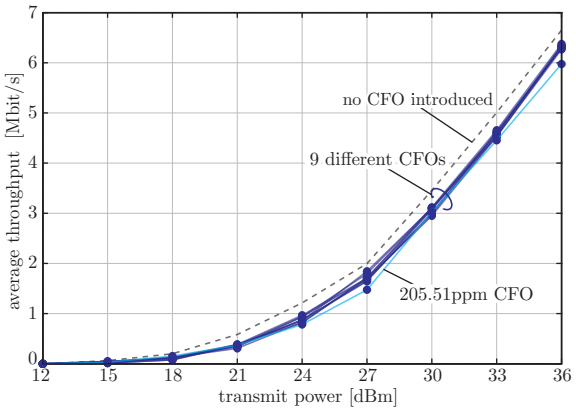

Fig. 4. Throughput of the nine different CFOs in Table 1.

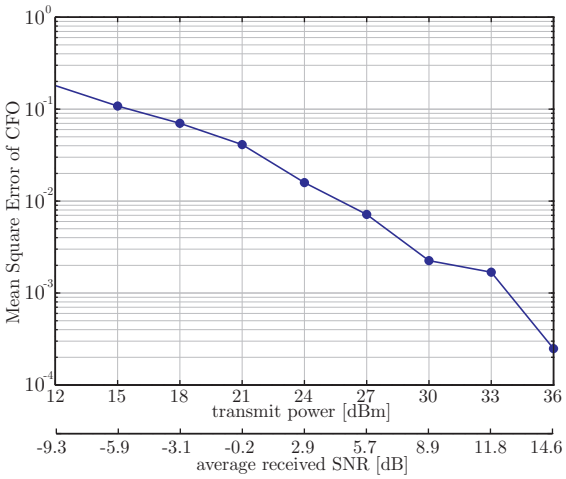

Fig. 5. Mean Square Error over transmit power.

(MSE) curve is obtained in Fig. 5. When calculating the MSE, the IFO is assumed to be perfectly corrected. Thus, only the error from the FFO and the RFO estimation is considered. It can be seen that the estimation error decreases proportionally with increasing transmit power in dBm.

In Fig. 6, we fix the transmit power and the CFO at a certain level to observe the estimated CFOs and the received SNRs over 110 channel realizations. The estimated result varies significantly with the fluctuation of the instantaneous SNR, in particular in the low SNR region.

4.3. Physical-layer Throughput

The resulting throughput curves of the three pilot-based RFO compensation schemes are shown in Fig. 7. The

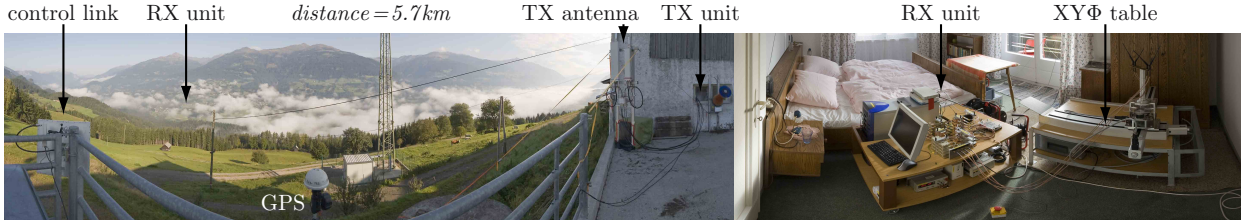

Fig. 3. Measured Scenario (use PDF to zoom).

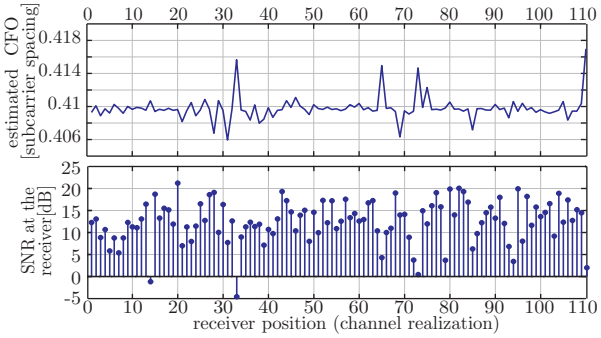

Fig. 6. Estimated CFO at transmit power 36 dBm, $\varepsilon = 0.41$ subcarrier spacing.

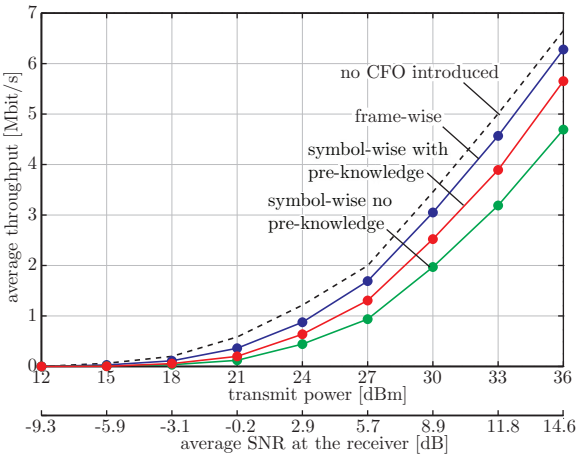

Fig. 7. Average throughput of pilot-based approaches.

best among the three is the frame-wise one, having only 1 dB loss to the ideal case. For the symbol-wise methods, when the pre-knowledge is not considered, the loss can be up to 3 dB. Although the initial estimate from the previous frame provides 1 dB gain, it is not as much as that was claimed in [4]. This can be attributed to the fluctuation of the instant SNR at the receiver (Fig. 6), which makes the estimate from the previous frame less reliable.

The throughput gain brought by the data subcarriers can be seen in Fig. 8. A throughput curve of the genie-driven solution is given as a reference, where all the data symbols are assumed to be demapped correctly. Compared to the pilot-based approach, the overall gain is around 3 dB. However, it has to be noticed that the data-aided approach is data dependent. In the low SNR region, where smaller symbol alphabets are used, the data-aided method performs quite well, while the loss becomes larger for higher SNRs where larger symbol alphabets are employed adaptively.

5. CONCLUSION

In this work, we present WiMAX measurement results of transmissions with compensated CFOs. The throughput results show that the estimation from the previous frame is not fully reliable for the current frame. The data-aided method effectively compensates the loss in throughput caused by the CFO at lower SNRs, while at

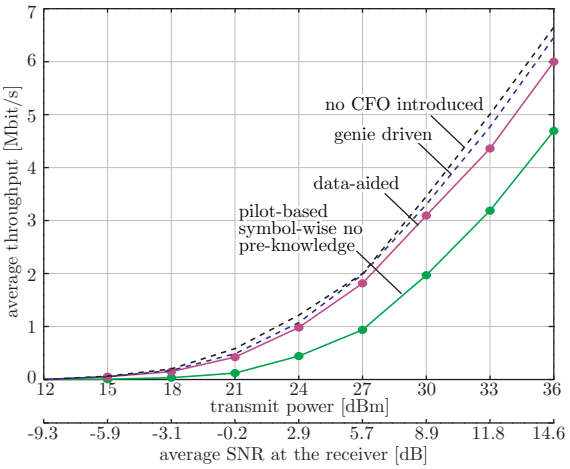

Fig. 8. Average throughput of the data-aided approach.

higher SNRs there is still room for improvement.

6. ACKNOWLEDGEMENT

Funding for this research was provided by the fFORTE WIT - Women in Technology Program of the Vienna University of Technology. This program is co-financed by the Vienna University of Technology, the Ministry for Science and Research and the fFORTE Initiative of the Austrian Government. Part of the funding was also provided by the Christian Doppler Laboratory for Wireless Technologies for Sustainable Mobility.

References

[1] J. J. van de Beek, M. Sandell, and P. O. Borjesson, "ML estimation of time and frequency offset in OFDM system," *IEEE Transactions on Signal Processing*, vol. 45, pp. 1800–1805, Jul. 1997.

[2] M. Speth, S. Fechtel, G. Fock, and H. Meyr, "Optimum receiver design for OFDM-based broadband transmission. II. a case study," vol. 49, pp. 571–578, Apr 2001.

[3] K. Shi, E. Serpedin, and P. Ciblat, "Decision-directed fine synchronization in OFDM systems," *IEEE Transactions on Communications*, vol. 53, pp. 408–412, March 2005.

[4] Q. Wang, C. Mehlführer, and Rupp M., "SNR optimized residual frequency offset compensation for WiMAX with throughput evaluation," in *Proc. 17th European Signal Processing Conference (EUSIPCO 2009)*, Aug. 2009.

[5] S. Caban, C. Mehlführer, R. Langwieser, A. L. Scholtz, and M. Rupp, "Vienna MIMO testbed," *EURASIP Journal on Applied Signal Processing, Special Issue on Implementation Aspects and Testbeds for MIMO Systems*, 2006.

[6] S. Caban, C. Mehlführer, G. Lechner, and M. Rupp, ""Testbedding" MIMO HSDPA and WiMAX," in *Proc. 70th IEEE Vehicular Technology Conference (VTC2009-Fall)*, Sept. 2009.

[7] "http://www.nt.tuwien.ac.at/fileadmin/data/testbed /Carinthia-RX-TX-GPS.kmz," .

[8] IEEE, "IEEE standard for local and metropolitan area networks; part 16: Air interface for fixed broadband wireless access systems, IEEE Std. 802.16-2004," Oct. 2004.

[9] C. Mehlführer, S. Caban, and M. Rupp, "Experimental evaluation of adaptive modulation and coding in MIMO WiMAX with limited feedback," *EURASIP Journal on Advances in Signal Processing, Special Issue on MIMO Systems with Limited Feedback*, 2008.